Analytical Investigation on Joule-Thomson Micro-Cryocoolers

N. Tzabar

Rafael
Haifa, Israel 3102102

ABSTRACT

Joule-Thomson (JT) cryocoolers include recuperative heat exchangers (RHE) where a high pressure fluid is cooled by the same fluid in a state of lower pressure and temperature. The pressure and temperature differences between the streams are in the order of a few MPa and hundreds of K, respectively.

The RHE is the largest component of the JT cryocooler cold-end; therefore, miniaturization of the cooler may be achieved with a micro-fabricated RHE. Our preliminary design of a micro JT cryocooler is based on a plane counter flow micro RHE (μRHE) that consists of straight micro-channels for both high and low pressure streams. An analytical quasistatic model of the cryocooler has been developed for investigating the μRHE performances. The analysis calculates five temperature profiles in the RHE; high and low pressure streams, both stream covers, and the buffering material between the streams. The μRHE model is further developed for a complete micro JT cryocooler at transient conditions. This analytical model helps to design the prototypes to be fabricated and tested and facilitates parameter and sensitivity studies. Some preliminary results of the parameter study are presented and discussed.

INTRODUCTION

Joule-Thomson (JT) cryocoolers are suitable for cooling small electronic devices that operate at cryogenic temperatures. The cold stage size of mini JT cryocoolers that consist of finned-tube, tube-in-tube, sintered, or similar heat exchangers is already small compared to other cryocoolers and benefit from the absence of moving parts, vibrations, and heat emission. Further improvement in JT cold stages can be achieved by implementing the recuperative heat exchanger (RHE) in micro fabrication techniques to obtain further miniaturization. In addition to the clear advantage of miniature dimensions, micro JT cryocoolers also gain low intrinsic heat load and heat capacity.

William A. Little [1,2] established the MEMS based JT cryocoolers employing flat plate micro recuperative heat exchangers (μRHE) that consist of straight and winding micro-channels. Mikulin et al. [3] experimentally investigated several plane μRHE and a disk plate cooler with Archimedean spiral channel. Narayanan and Venkatarathnam [4,5] performed numerical analysis on winding channel heat exchangers taking into account the conductive heat transfer in the solids and came to the conclusion that there is an optimum balance between the parasitic heat leak of the μRHE and the heat transfer between the streams. Much effort is invested at the University of

Cryocoolers 18, edited by S.D. Miller and R.G. Ross, Jr.

Twente on flat plane micro JT cryocoolers [6] and several configurations of micro cryocoolers have been developed, analyzed, and tested for various cooling temperatures and with different working fluids. A larger heat exchanger that still consists of micro-channels is developed at KAIST [7] where a technique for lowering the axial heat leaks is developed. Whith et al. [8] developed a multi layer μRHE with a cubic shape for cryosurgical probes and a tubes-in-tube μRHE is developed by NIST and the University of Colorado at Boulder [9-11].

Designing a micro-cryocooler and improving its efficiency requires developing the ability to analyze the μRHE, the complete cryocooler, and to perform parametric investigations. Several groups developed numerical models of μRHE and micro JT cryocoolers; Nellis [12] developed a finite differences model of a general heat exchanger with exponentially distributed grid that is verified against analytical solutions. Foli et al. [13] numerically investigated μRHE and show the trade-off between minimal pressure drops and maximal heat transfer. Lerou et al. [14] optimized a flat μRHE using finite element method to minimize the entropy generation. Cao et al. [15] used this model to further optimize a two stage micro JT cooler.

In the present research a steady state model of flat μRHE is developed, expressed with linear algebraic set of equations that are analytically solved. The model determines five temperature profiles; high pressure stream, low pressure stream, buffering material, high pressure cover, and low pressure cover. The model neglects the radiation heat transfer and the dependence of material properties on temperature, in order to maintain the equations' linearity. The model is further developed for transient conditions of a complete micro JT cryocooler. The transient model incorporates the radiation heat transfer and the dependence of material properties on temperature in a manner that preserves the analytical solution method.

RECUPERATIVE HEAT EXCHANGER CONFIGURATION

The μRHE of interest consists of three layers with straight parallel micro-channels for both high and low pressure streams, where the middle layer buffers between the two streams. A section of the μRHE that includes a single micro-channel for each stream is schematically described in Figure 1. The top layer, marked with 'A', includes the micro-channels of the high pressure stream, marked with 'H', where the layer thickness is y_A and the micro-channel depth is y_H. The layer at the bottom, marked with 'C', includes the micro-channels of the low pressure stream, marked with 'L', where the layer thickness is y_C and the micro-channel depth is y_L. The middle layer, marked with 'B', is the buffering layer between the two streams, with thickness of y_B. Both channels width and length are W and L, respectively. The wall thickness between two channels of the same stream equals W_{wall}; therefore, the section in Figure 1 includes walls of $\frac{1}{2}W_{wall}$ at the channel sides.

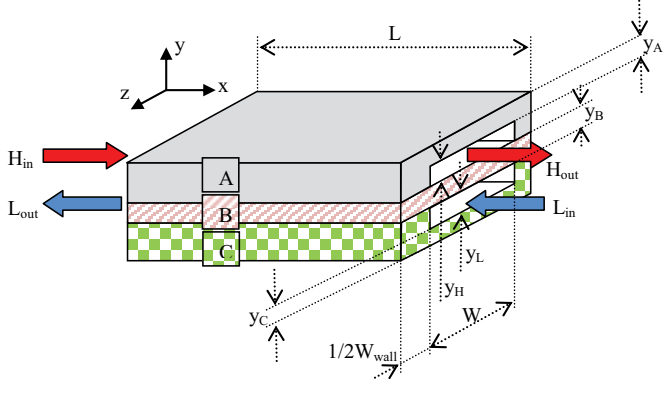

Figure 1. A schematic of the μRHE.

ANALYTICAL MODEL

μRHE model at steady state

The analytical model refers to a section of a single channel for the high pressure stream and another single channel for the low pressure streams, as described in Figure 1. The model assumes heat transfer, conduction and convection, among all parts at the y direction, axial (x direction) conduction heat transfer in layers A, B, and C, and no heat transfer at the z direction. Under these assumptions, the current model is suitable for analyzing multi channels heat exchangers as well. In order to obtain a linear set of equations that can be analytically solved the radiation heat transfer is neglected and all material properties are assumed to be constants. The μRHE is divided into N equal elements along the x axis, where the length of each element is $\Delta x = L / N$. The position of each element along the μRHE is presented by the index i where i = 1 at the warm end and i = N at the cold end. Figure 2 shows a schematic of the model with the heat and enthalpy flows, $\dot{Q}$ and $\dot{H}$, respectively. In each element there are 5 parts; A, H, B, L, and C, with a single energy balance equation for each part; therefore, totally there are 5N equations that describe the μRHE. The equations for element i are:

$$\dot{Q}_A^i = \dot{Q}_A^{i+1} + \dot{Q}_{AH}^i \tag{1}$$

$$\dot{H}_H^i + \dot{Q}_{AH}^i = \dot{H}_H^{i+1} + \dot{Q}_{HB}^i \tag{2}$$

$$\dot{Q}_B^i + \dot{Q}_{HB}^i = \dot{Q}_B^{i+1} + \dot{Q}_{BL}^i \tag{3}$$

$$\dot{H}_L^{i+1} + \dot{Q}_{BL}^i + \dot{Q}_{CL}^i = \dot{H}_L^i \tag{4}$$

$$\dot{Q}_C^i = \dot{Q}_C^{i+1} + \dot{Q}_{CL}^i \tag{5}$$

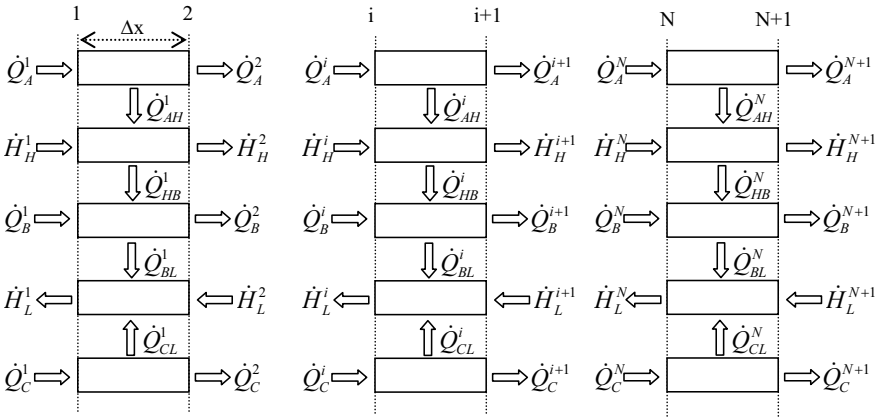

Figure 2. A schematic of the analytical model with the heat and enthalpy flows.

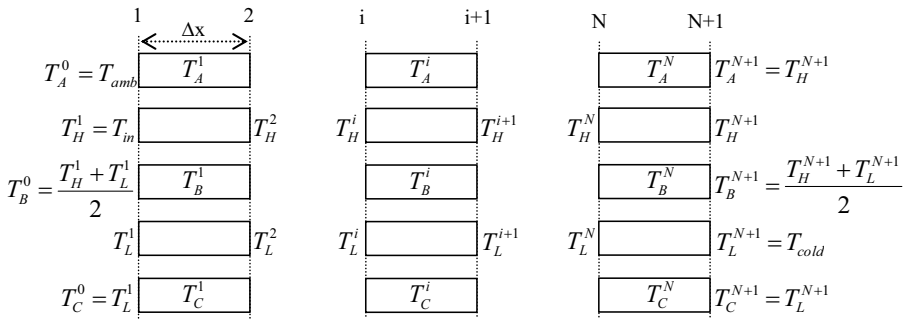

Figure 3. A schematic of the analytical model with the unknown temperatures.

In a more detailed expression, the equations of element i become:

$$\frac{k_A A_{A\perp}}{\Delta x/2}\left(T_A^{i-1}-T_A^i\right)=\frac{k_A A_{A\perp}}{\Delta x/2}\left(T_A^i-T_A^{i+1}\right)+\alpha_{AH}A_{AH}\left(T_A^i-\frac{T_H^i+T_H^{i+1}}{2}\right) \tag{6}$$

$$\dot{m}_H c_{p,H}^i T_H^i+\alpha_{AH}A_{AH}\left(T_A^i-\frac{T_H^i+T_H^{i+1}}{2}\right)=\dot{m}_H c_{p,H}^{i+1}T_H^{i+1}+\alpha_{HB}A_{HB}\left(\frac{T_H^i+T_H^{i+1}}{2}-T_B^i\right) \tag{7}$$

$$\frac{k_B A_{B\perp}}{\Delta x/2}\left(T_B^{i-1}-T_B^i\right)+\alpha_{HB}A_{HB}\left(\frac{T_H^i+T_H^{i+1}}{2}-T_B^i\right)=\frac{k_B A_{B\perp}}{\Delta x/2}\left(T_B^i-T_B^{i+1}\right)+\alpha_{BL}A_{BL}\left(T_B^i-\frac{T_L^i+T_L^{i+1}}{2}\right) \tag{8}$$

$$\dot{m}_L c_{p,L}^{i+1}T_L^{i+1}+\alpha_{BL}A_{BL}\left(T_B^i-\frac{T_L^i+T_L^{i+1}}{2}\right)+\alpha_{CL}A_{CL}\left(T_C^i-\frac{T_L^i+T_L^{i+1}}{2}\right)=\dot{m}_L c_{p,L}^i T_L^i \tag{9}$$

$$\frac{k_C A_{C\perp}}{\Delta x/2}\left(T_C^{i-1}-T_C^i\right)=\frac{k_C A_{C\perp}}{\Delta x/2}\left(T_C^i-T_C^{i+1}\right)+\alpha_{CL}A_{CL}\left(T_C^i-\frac{T_L^i+T_L^{i+1}}{2}\right) \tag{10}$$

where k is the conductive heat transfer coefficient, c_p is the specific heat capacity, and $A_\perp$ is a cross section area on a y-z plane of the solid indicated by the attached subscript. $\dot{m}_H$ and $\dot{m}_L$ are the mass flow rates of the high and low pressure fluids, respectively, and $A_{\beta\delta}$ is an area on a x-z plane between part 'β' and part 'δ'. $\alpha_{\beta\delta}$ is the convective heat transfer coefficient between part 'β' and part 'δ' calculated as follows [16]:

$$\alpha=8.235\left(1-2.042\chi+3.0853\chi^2-2.4765\chi^3+1.0578\chi^4-0.1861\chi^5\right) \tag{11}$$

where χ = channel height / channel width

The unknowns in the equations are the temperatures that are detailed in Figure 3. The temperature of the solids, A, B, and C, are constants per element where for a fluid part in an element, H and L, there are two temperatures at the edges. In addition, every solid has two additional temperatures at the edges; thus, there are N+2 unknowns for each solid and N+1 unknowns for each fluid which make totally 5N+8 unknowns. The extra 8 equations are derived from the end conditions that are specified in Figure 3, where T_{amb} is the ambient temperature, T_{in} is the temperature of the incoming high pressure fluid, and T_{cold} is the temperature of the incoming low pressure fluid, all provided to the model. This set of equations is solved analytically and provides five temperature profiles in the μRHE; two streams, H and L, two solid covers, A and C, and the buffering layer, B. After obtaining the temperature profiles the pressure drops of the fluids are calculated. For every element the pressure drop is calculated by [16]:

$$\Delta p=f\frac{\Delta x}{D_h}\frac{1}{2}\rho v_m^2 \tag{12}$$

$$f=\frac{1}{\mathrm{Re}}\left[-0.3882\left(\frac{1}{\chi}\right)^2+7.4174\left(\frac{1}{\chi}\right)+49.533\right] \tag{13}$$

$$\mathrm{Re}=\frac{v_m D_h}{\upsilon} \tag{14}$$

where D_h is the hydraulic diameter, ρ is the density, v_m is the mean flow velocity, and υ is the kinematic fluid velocity. The pressure drop is determined from element 1 to element N, where the fluid properties are obtained from REFPROP™ as a function of the element temperature and the element inlet pressure that equals the previous element outlet pressure. Finally, the effectiveness of the μRHE is calculated as follows:

$$\varepsilon=\frac{h_{L,out}-h_{L,in}}{h_{H,in}'-h_{L,in}}\quad;\quad h_{H,in}'=h\left(T_{H,in},p_{L,out}\right) \tag{15}$$

JT cryocooler model at transient conditions

The steady state model of the μRHE that is described above is further developed to a transient model of a complete JT cryocooler that is described in Figure 4. The high pressure fluid that leaves the μRHE enters an expansion valve where its pressure drops together with its temperature, according to the JT coefficient. The fluid that leaves the expansion valve enters an evaporator where it absorbs heat from the device that has to be cooled. The evaporator outgoing fluid enters the low pressure port of the μRHE.

The operation of the cryocooler is divided into equal time intervals, Δt, where in each interval the μRHE is solved at a steady state. The main parameter that is changed with the intervals is T_4 (equals T_{cold} mentioned in Figure 3), which is the temperature of the fluid that leaves the evaporator and enters the low pressure port of the μRHE. The temperature of the fluid that enters the evaporator, T_3, is determined by REFPROP as a function of pressure and enthalpy; the pressure is the low pressure in the cycle and the enthalpy equals the enthalpy at point 2. The enthalpy of the fluid that leaves the evaporator, h_4, is calculated as follows:

$$\dot{H}_4 \cdot \Delta t = \left(\dot{H}_3 + \dot{Q}_A + \dot{Q}_B + \dot{Q}_C + \dot{Q}_{RHE,rad} + \dot{Q}_{evapoator}\right)\Delta t + Q_{RHE,C_p} + C_{evaporator} \cdot \Delta T_{evaporator} \quad (16)$$

where $\dot{H}_3$ and $\dot{H}_4$ are the enthalpy of the fluids entering and leaving the evaporator, respectively, $\dot{Q}_A$, $\dot{Q}_B$, and $\dot{Q}_C$ are the heat loads of the three layers of the μRHE, $\dot{Q}_{evaporator}$, $C_{evaporator}$, and $\Delta T_{evaporator}$ are the heat load, heat capacity, and temperature difference between time intervals of the evaporator. $\dot{Q}_{RHE,rad}$ is the radiation heat load on the μRHE that is ignored at the steady state model. It is calculated after every time step according to the previous temperature profiles:

$$\dot{Q}^j_{RHE,rad} = \varepsilon\sigma \sum_{i=1}^{N} \left[A_{A,i} \left(T_{amb}{}^4 - T^{j-1}_{A,i}{}^4 \right) + A_{C,i} \left(T_{amb}{}^4 - T^{j-1}_{C,i}{}^4 \right) \right] \quad (17)$$

where ε is the emissivity and σ is the Stefan-Boltzmann's constant. The subscript index i indicates the element number along the x axis and the superscript index j indicates the time step. A_A and A_C is the area exposed to radiation heat transfer of parts A and C, respectively. In addition, all the materials properties that were assumed to be constants at the steady state model become temperature dependent. For each element at every time step the properties are taken as a function of its temperature at the previous time step.

The flow rate in the cryocooler is governed by the expansion valve. The expansion valve is characterized by the free flow rate (FFR) parameter which equals the nitrogen flow rate at pressure of 6.9 MPa (1000 psi) and temperature of 296 K. The actual flow rate during the cryocooler operation at time step j+1 is determined as follows:

$$\dot{m}^{j+1} = FFR \cdot C \cdot \frac{p^j_{H,i=N}}{6.9} \sqrt{\frac{296}{T^j_{H,i=N}}} \quad (18)$$

where the pressure is in MPa and the temperature is in K. C is a coefficient depends on the temperature and pressure in the expansion valve inlet and is provided in a pre determined table.

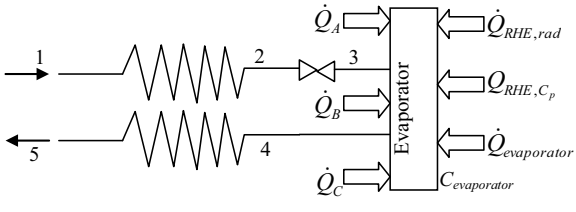

Figure 4. The model of a complete JT cryocooler.

RESULTS AND DISCUSSION

µRHE model at steady state

Five temperature profiles are presented in Figure 5 for a µRHE with length of 30 mm, width of 9 mm, and W_{wall} equals 0.2 mm. The thickness of solids A, B, and C are 0.2, 0.1, and 0.15 mm, respectively. The high and low pressure channel heights are 0.05 and 0.1 mm, respectively. The fluid is nitrogen at 10 MPa and 0.2 MPa in the high and low pressure streams, respectively, and the flow rate equals 0.02 g/s. The high pressure fluid enters the µRHE at 300 K and the low pressure fluid enters the µRHE at 80 K. The dashed lines refer to the fluids and the continuous lines present the solids. Strength calculations are not taken into account in the current model.

The temperature profiles enable to determine the effectiveness of the heat exchanger, the temperatures of the outgoing fluids, the conductive heat transfer at the x axis through the solids, and the pressure drops at both high and low pressure streams. Since the model is analytically solved, there are no convergence problems and other running limitations. Therefore, a wide parametric analysis is feasible targeting optimization of the µRHE design against different purposes. Figure 6 presents the dependence of the effectiveness on the number of elements and shows that using 500 elements provides suitable accuracy. 500 elements mean element length of 0.06 mm that is in the same order of magnitude of the channel heights; therefore, it becomes the suggested number of elements. The influence of the channels height on the effectiveness and pressure drops are presented in Figure 7. Decrease in both channel heights increases the µRHE effectiveness and the pressure drops at both streams. Figure 7 (b) shows the limits where the pressure drops become significantly high. In our current example, the high and low pressure channel heights shall not go down below 0.05 and 0.1 mm, respectively. The influence of the µRHE length and width on its effectiveness and parasitic heat load is presented in Figure 8. As expected, longer µRHE has improved effectiveness and reduced parasitic heat load; however, short µRHE is desirable due to miniaturization considerations. Wider channels provide higher heat transfer area and an increased effectiveness; however, besides the desire for miniature µRHE, the width of the channel shall be minimized in order to decrease the parasitic heat load. Figure 8 (b) shows a significant relation between the channels width and the parasitic heat load which convinces that a minimum channel width is preferable. Surprisingly, narrow channels do not have higher pressure drops, even though the velocity is increased, since the friction factor depends on the channel aspect ratio (see equation 13). Finally, Figure 9 presents the effectiveness as a function of the flow rate. It is clear that the current µRHE is designed for flow rates up to about 0.02 g/s and increased flow rates reduce the effectiveness significantly.

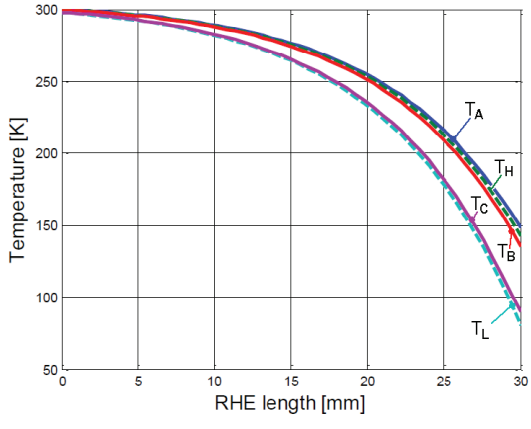

Figure 5. Temperature profiles in the µRHE at steady state. Solid temperatures are presented in solid lines and fluid temperatures are presented in dashed lines.

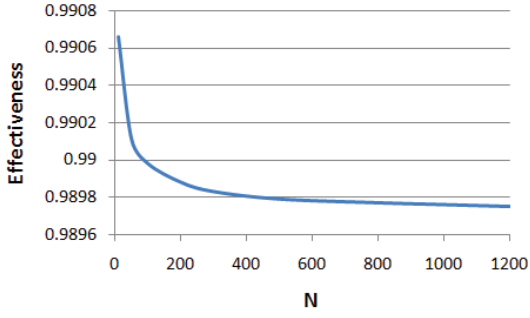

Figure 6. µRHE effectiveness dependence on the number of elements.

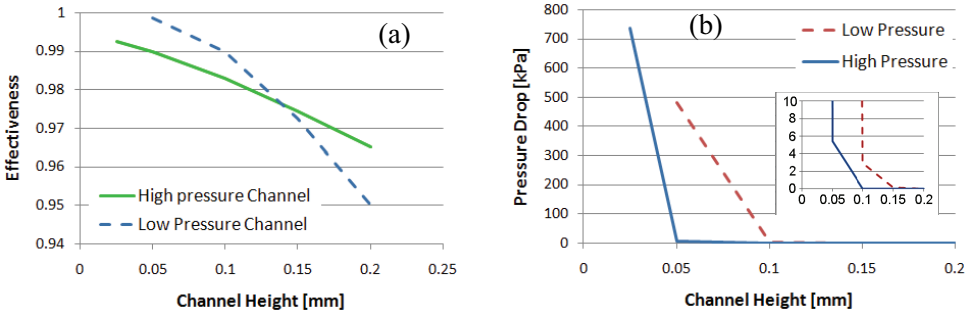

Figure 7. Channel heights influence on (a) µRHE effectiveness (b) pressure drops.

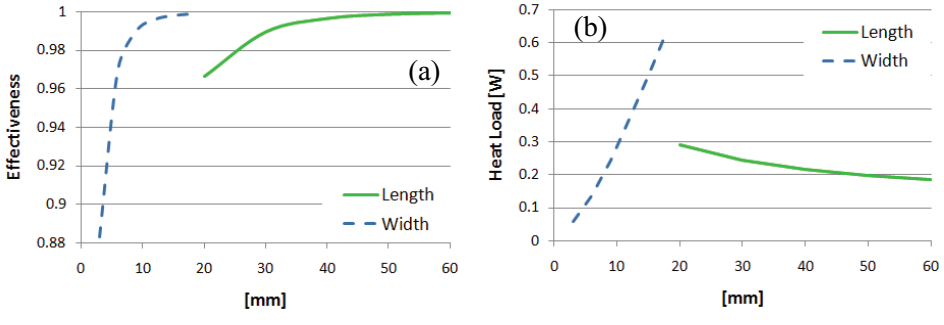

Figure 8. µRHE length and width influence on its (a) Effectiveness (b) Parasitic heat load.

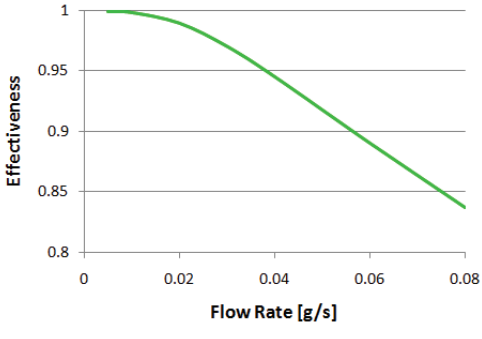

Figure 9. µRHE effectiveness as a function of the flow rate.

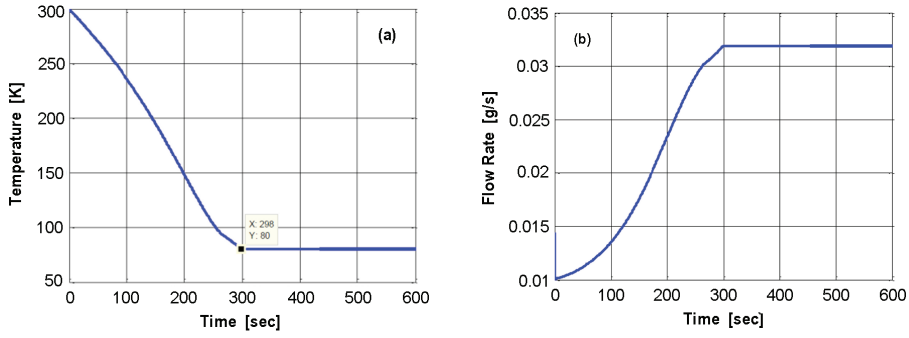

Figure 10. Cool down process of a complete JT cryocooler; (a) temperature cool down, (b) flow rate.

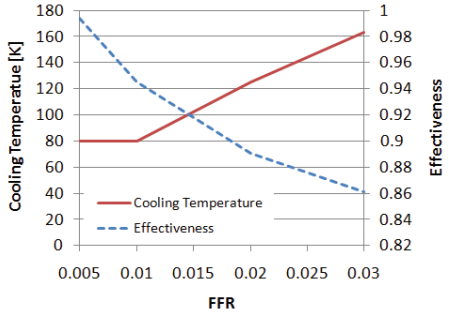

Figure 11. Cooling temperature and μRHE effectiveness as a function of FFR of a JT cryocooler.

JT cryocooler model at transient conditions

The investigation of the complete JT cryocoolers refers to the basic parameters that are detailed in the beginning of this chapter. The main difference is in the definition of the flow rate. Since the flow rate changes during the cool down process, we define the expansion valve with the FFR parameter that in the current case equals 0.01. Figure 10 (a) presents the cool down process of the basic configuration. The initial flow rate is 0.01 g/s and it increases to 0.032 g/s at the end of the cool down process, as shown in Figure 10 (b). The influence of FFR on the JT cryocooler performances is presented in Figure 11. The cooling temperature is presented in solid line and the effectiveness is presented in dashed line. At low flow rates the cryocooler reaches the cooling temperature target of 80 K; however, when the flow rate increases the μRHE effectiveness decreases until it becomes insufficient and the final cooling temperature increases. In the current case the upper limit of the flow rate to attain cooling temperature of 80 K is FFR=0.01 which yields μRHE effectiveness of 0.945.

Figure 12 shows the cooling temperature in solid line, the effectiveness in dashed line, and the cool-down time in dotted line, as a function of the μRHE length. From miniaturization aspects the shortest μRHE is desirable; however, Figure 12 proves that there is a low limit for the length where under it the μRHE effectiveness is inferior and the cryocooler does not reach the cooling target of 80 K. Beyond this limit, an increase of the μRHE length increases the effectiveness and improves the cool down time. The significant dependence of the cool down time on the channel heights is presented in Figure 13; solid line for high pressure channel and dashed line for low pressure channel. The lower limits for the channel heights are obtained from the μRHE steady state study to avoid high pressure drop, see Figure 7 (b). The results presented up to channel heights of 0.15 mm since above it the effectiveness drops and the cryocooler does not reach the cooling temperature of 80 K.

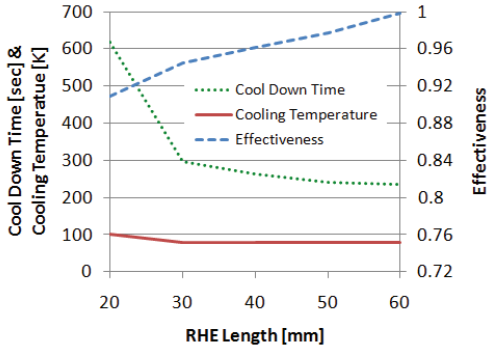

Figure 12. Cooling temperature, cool down time, and effectiveness as a function of the μRHE length.

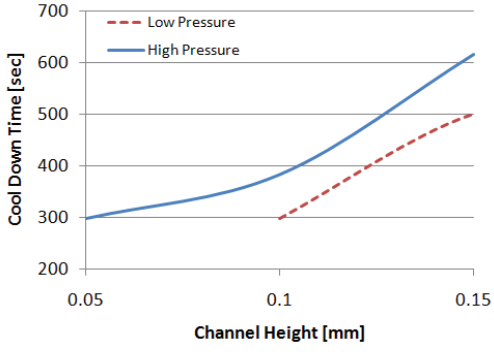

Figure 13. Cool down time as a function of channel heights.

CONCLUSIONS

A numerical model has been developed for analyzing the performance of micro JT cryocoolers. The complete model is based on a steady state parametric model of a μRHE that consists of a set of linear equations. This set of equations is analytically solved, thus, there are no convergence problems or illegal solutions. Therefore, an extensive parametric investigation is feasible in a very convenient manner. The model calculates five temperature profiles in the μRHE to obtain the axial heat leaks and radiation heat loads. The linearity of the μRHE steady state model is obtained by neglecting the radiation heat transfer and assuming constant material properties.

An advanced transient model of a complete micro JT cryocooler that is based on the steady state model is further developed. The transient model incorporates the radiation heat transfer and material properties temperature dependence in a manner that preserves the analytical solution.

The small dimensions of the μRHE reinforce high sensitivity of its performances to the geometry and operating conditions. The μRHE effectiveness is a significant parameter that is used to examine the performance of the micro JT cryocooler. For the current case, when the effectiveness decreases below about 94 % the cryocooler does not reach the desired cooling temperature of 80 K. The model described in this paper provides a convenient tool for designing micro JT cryocooler by examining trends and sensitivities of parameters. The results comply with published data and are going to be validated against experimental results.

REFERENCES

1. Little W.A., "Microminiature refrigeration", *Rev. of Science Instrum*ents, vol. 55(1984), pp. 661-679.

2. Little W.A., "Microminiature refrigeration", *Advances in Cryogenic Eng*ineering, vol. 53(2008), pp. 597-605.
3. Mikulin E., Shevich J., Danilenko T., Solovov N., and Veselov V., "The miniature Joule-Thomson Refrigerator", *Cryogenics*, vol. 32(1992), pp. 17-19.
4. Narayanan S.P. and Venkatarathnam G., "Performance of a counterflow heat exchanger with heat loss through the wall at the cold end", *Cryogenics*, vol. 39(1999), pp. 43-52.
5. Narayanan S.P. and Venkatarathnam G., "Analysis of performance of heat exchangers used in practical micro miniature refrigerators", *Cryogenics*, vol. 39(1999), pp. 517-527.
6. Derking J.H., Holland H.J., Lerou P.P.P.M., Tirolien T., and ter Brake H.J.M., "Micromachined Joule-Thomson cold stages operating in the temperature range 80 – 250 K", *International Journal of Refrigeration*, vol. 35(2012), pp. 1200-1207.
7. Baek S., Kim J.H., Jeong S., and Jung J., "Development of highly effective cryogenic printed circuit heat exchanger (PCHE) with low axial conduction", *Cryogenics*, 52(2012), pp. 366-374.
8. White M.J., Zhu W., Nellis G.F., Klein S.A., and Gianchandani Y.B., "Performance of a MEMS heat exchanger for cryosurgical probe", *Cryocoolers*, vol. 15(2009), pp. 387-395.
9. Lin M.H., Bradley P.E., Huber M.L., Lewis R., Radebaugh R., and Lee Y.C., "Mixed refrigerants for a glass capillary micro cryogenic cooler", *Cryogenics*, vol. 50(2010), pp. 439-442.
10. Bradley P.E., Radebaugh R., Lewis R.J., Lin M.H., and Lee T.C., "Temperature instability comparison of micro- and meso- scale Joule-Thomson cryocoolers employing mixed refrigerants", *Advances in Cryogenic Eng*ineering, vol. 57(2012), pp. 690-697.
11. Lewis R., Wang Y., Schneider H., Lee Y.C., and Radebaugh R., "Study on mixed refrigerant undergoing pulsating flow in micro coolers with pre-cooling", *Cryogenics*, vol. 57(2013), pp. 140-149.
12. Nellis G.F., "A heat exchanger model that includes axial conduction, parasitic heat loads, and property variations", *Cryogenics*, vol. 43(2003), pp. 523-538.
13. Foli K., Okabe T., Olhofer M., Jin Y., and Sendhoff B., "Optimization of micro heat exchanger: CFD, analytical approach and multi-objective evolutionary algorithms", *International Journal of Heat and Mass Transfer*, vol. 49(2006), pp. 1090-1099.
14. Lerou P.P.P.M., Veenstra T.T., Burger J.F., ter Brake H.J.M., and Holland H.J., "Optimization of counterflow heat exchanger geometry through minimization of entropy generation", *Cryogenics*, vol. 45(2005), pp. 659-669.
15. Cao H.S., Mudaliar A.V., Derking J.H., Lerou P.P.P.M., Holland H.J., Zalewski D.R., Vanapalli S., and ter Brake H.J.M., "Design and optimization of a two-stage 28 K Joule-Thomson microcooler", *Cryogenics*, vol. 52(2012), pp. 51-57.
16. Holman J.P., Heat transfer. 7th ed., McGraw-Hill, New York (1990), p. 291.